Available online at www.sciencedirect.com
ScienceDirect
Bioorganic & Medicinal Chemistry 16 (2008) 3565–3579
Bioorganic & Medicinal Chemistry

Computational analysis of the binding affinities of the natural-product cyclopentapeptides argifin and argadin to chitinase B from *Serratia marcescens*

Hiroaki Gouda,[a,*] Yuichi Yanai,[a] Akihiro Sugawara,[b] Toshiaki Sunazuka,[b,c] Satoshi Ōmura[b,c] and Shuichi Hirono[a]

[a]*School of Pharmaceutical Sciences, Kitasato University, 5-9-1 Shirokane, Minato-ku, Tokyo 108-8641, Japan*
[b]*Kitasato Institute for Life Sciences and Graduate School of Infection Control Sciences, 5-9-1 Shirokane, Minato-ku, Tokyo 108-8641, Japan*
[c]*The Kitasato Institute, 5-9-1 Shirokane, Minato-ku, Tokyo 108-8642, Japan*

Received 10 January 2008; revised 4 February 2008; accepted 5 February 2008
Available online 8 February 2008

Abstract—Molecular dynamics (MD) simulations and the molecular mechanics Poisson–Boltzmann surface area (MM-PBSA) method were applied to study the interaction of the natural-product cyclopentapeptide chitinase inhibitors argifin and argadin with chitinase B (ChiB) from *Serratia marcescens*. Argadin inhibited ChiB with an inhibition constant (K_i) value of 20 nM, which was three orders of magnitude greater than that of argifin (K_i = 33,000 nM). The MM-PBSA free-energy analysis provided absolute binding free energies of −6.98 and −11.16 kcal/mol for the argifin and argadin complexes, respectively. These estimates were in good agreement with the free energies derived from the experimental K_i values (−6.36 and −10.92 kcal/mol for the argifin and argadin complexes, respectively). The energetic analysis revealed that the van der Waals and nonpolar solvation energies drove the binding of both argifin and argadin. We found that the binding of argadin gained ~12 kcal/mol more van der Waals energy than that of argifin, which was mainly responsible for the difference in binding free energy between argifin and argadin. In particular, W220 and W403 of ChiB were found to contribute to the more favorable van der Waals interaction with argadin. We also designed argifin derivatives with better binding affinity, in which a constituent amino-acid residue of argifin was mutated to one with a bulky side chain. The derivative in which D-Ala of argifin was replaced with D-Trp appeared to possess a binding affinity that was equally potent to that of argadin.

1. Introduction

Family 18 chitinases hydrolyze chitin, which is a linear polymer of β-(1,4)-linked *N*-acetyl-D-glucosamine (GlcNAc) and is one of the most abundant biopolymers in the biosphere. These enzymes are present in a wide range of organisms including bacteria, fungi, insects, mammals, and humans.[1–5] As chitin is a major structural component of fungi and insects, family 18 chitinases play important physiological roles in these organisms.[2,3,6,7] Chitinase inhibitors therefore have potential to function as fungicides and insecticides. In fact, they have been reported to inhibit the molting of *Periplaneta americana*[8] and to prevent *Candida albicans* from undergoing morphological change to the filamentous form, which has pathogenic characteristics.[9] Humans also have two family 18 chitinases: chitotriosidase and mammalian acidic chitinase.[4,5] Recently, it has been reported that mammalian acidic chitinase is implicated in triggering asthma.[10] This highlights a potentially important role for chitinase inhibitors as new anti-asthma medications. Several inhibitors of family 18 chitinases have been reported, the most potent being allosamidin, which is a pseudotrisaccharide isolated from the mycelium of *Streptomyces* sp.[11] Allosamidin exhibits strong inhibitory activity against family 18 chitinases (in the nanomolar range).[12,13] However, it seems to be an unsuitable compound for further development, because bulk synthesis of allosamidin and its

Keywords: Binding free energy; Drug design; Molecular dynamics; MM-PBSA.
* Corresponding author. Tel.: +81 3 3444 3548; fax: +81 3 3440 5246; e-mail: godah@pharm.kitasato-u.ac.jp

0968-0896/$ - see front matter © 2008 Elsevier Ltd. All rights reserved.
doi:10.1016/j.bmc.2008.02.017

derivatives is both difficult and expensive.[14] Other chitinase inhibitors, including styloguanidines,[15] cyclic dipeptides,[9,16] and psammaplins,[17] have also been reported. However, all of these inhibitors show only weak (high micromolar) inhibition.

Recently, two novel natural-product chitinase inhibitors, argifin[18] and argadin,[19] were isolated from *Gliocladium* and *Clonostachys* fungal cultures, respectively. Both argifin and argadin are cyclic pentapeptides, and their chemical structures are shown in Figure 1. In an initial test against chitinases from *Lucilia cuprina*, argifin, and argadin exhibited half-maximal inhibitory concentration (IC_{50}) values of 100 and 3.4 nM, respectively.[8,19] These inhibitors seem to be good candidates for the development of novel drugs, due to their potent inhibitory activity and synthetic accessibility by standard techniques in peptide chemistry. Argifin and argadin also inhibit a family-18 chitinase from *Serratia marcescens* (chitinase B or ChiB) with inhibition constant (K_i) values of 33,000 and 20 nM, respectively.[20] For both chitinases from *L. cuprina* and *S. marcescens*, argadin exhibits stronger inhibitory activity than that of argifin. In particular, argadin inhibition is three orders of magnitude stronger than argifin inhibition for ChiB. As argifin and argadin are highly similar in molecular structure and size, this is an interesting result, and elucidating the structural basis of the differential response could allow the characterization of a highly-specific ligand for novel drug development.

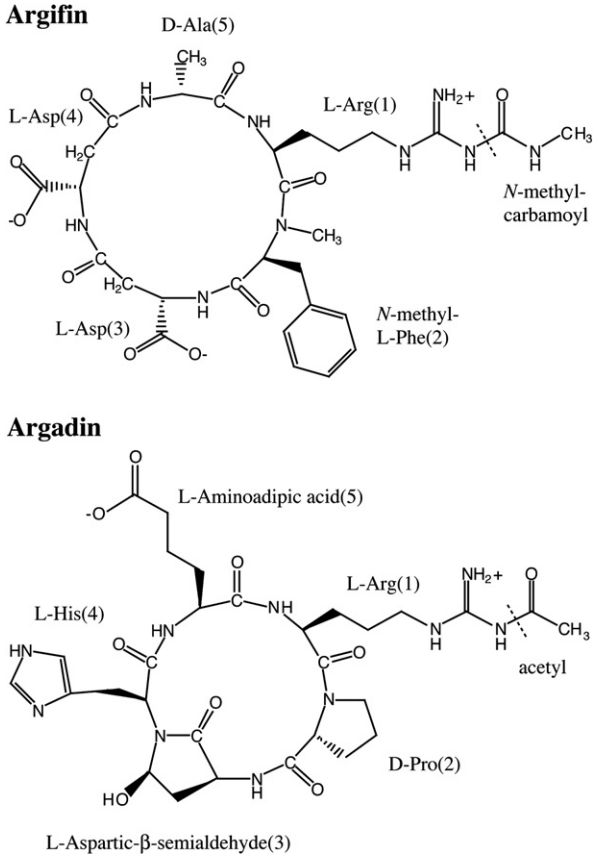

Figure 1. Chemical structures of argifin and argadin.

Recently, the three-dimensional structures of argadin and argifin in complex with ChiB have been determined by X-ray crystallography.[20] These structures have provided a detailed picture of the mode of interaction of argifin and argadin with ChiB, and have shown several differences in their binding. However, a quantitative analysis of the binding free energies of argifin and argadin with ChiB has so far remained lacking. In the current paper, the molecular mechanics Poisson–Boltzmann surface area (MM-PBSA) method[21] combined with molecular dynamics (MD) simulation is applied to study the binding affinities of argifin and argadin with ChiB. The MM-PBSA free-energy analysis has been successfully applied to a variety of protein–peptide, protein–ligand, and nucleic acid–ligand interactions.[22–28] The MM-PBSA method is not restricted to closely-related chemical structures, unlike the traditional free-energy perturbation (FEP) and thermodynamic-integration (TI) methods. Thus, it is a more suitable approach for studying the binding of argifin and argadin with ChiB, because assessment modeling by alchemical perturbation between argifin and argadin is not practical using the FEP and TI methods. A possible cause of the different binding affinities of argifin and argadin with ChiB was investigated here using the MM-PBSA method. We also examined the argifin derivatives that are predicted to possess better binding affinities than wild-type argifin. The information obtained from this analysis will be useful for further structure-based inhibitor design.

2. Results and discussion

2.1. Structural analysis of argifin–ChiB and argadin–ChiB complexes

The coordinates of the ChiB–argifin (code 1H0I) and ChiB–argadin (code 1H0G) complexes were obtained from the Protein Data Bank (PDB). Figure 2 shows the overall structures of argifin–ChiB (A) and argadin–ChiB (B) complexes. Each complex consists of a catalytic domain [residues 1–425 of ChiB and argifin(argadin)], a linker (residues 426–450 of ChiB), and a small carboxy (C)-terminal domain (residues 451–499 of ChiB). Figure 2 also indicates the hydrogen-bonding interactions of argifin (A) and argadin (B) with ChiB, as deduced from the X-ray crystal structures. Both argifin and argadin form hydrogen bonds with side chains of D142, E144, and Y214 located in the ChiB active site, which are conserved completely and required for catalytic activity in family 18 chitinases.[29,30] In addition, argifin forms one hydrogen bond with W97, and argadin forms two hydrogen bonds with D215 and R294. As shown in Figure 2, the orientation of the side chain of D142 is different in the argifin and argadin complexes: it points toward E144 in the argifin–ChiB complex (called as 'up' position), but toward D140 in the argadin–ChiB complex (called as 'down' position). As described in Section 4, we assumed that D142 was protonated in both argifin and argadin complexes, while E144 was protonated only in the latter.

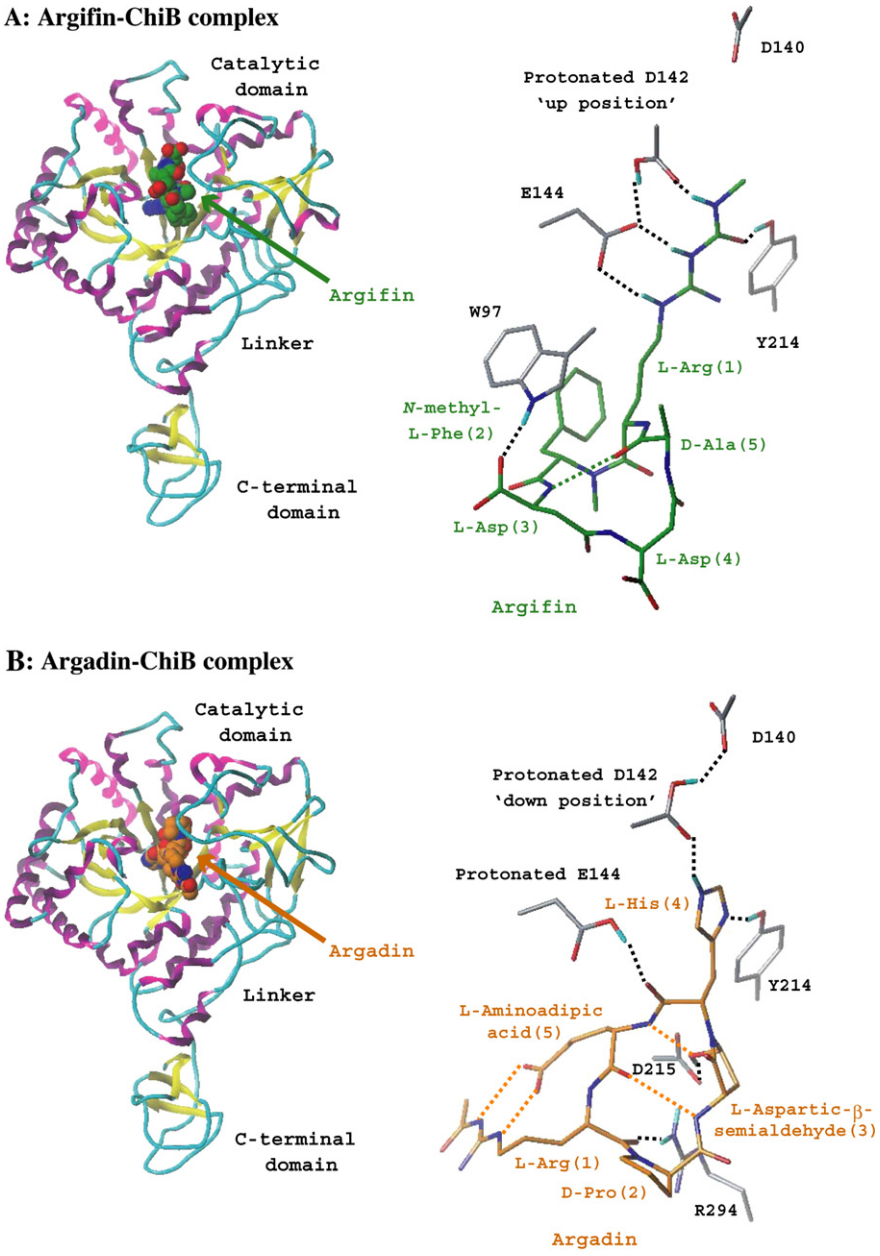

Figure 2. X-ray crystal structures of argifin–ChiB (A) and argadin–ChiB (B) complexes. The overall structure is shown on the left. The hydrogen-bonding interactions between argifin (argadin) and ChiB are indicated on the right by black dashed lines (only the hydrogen atoms involved in the interactions are displayed). The intra-molecular hydrogen bonds are also indicated by green (orange) dashed lines in the ChiB-bound conformation of argifin (argadin).

The MD simulations of 1700 ps length were performed using AMBER 7.0 package for both argifin and argadin complexes.[31] The root-mean-square deviation (RMSD) values relative to the initial structure were monitored along the entire MD trajectory of each complex. We calculated the RMSD values of all heavy atoms on the whole and for the subregions defined in Figure 2. Figure 3A plots the RMSD values on the whole, for the catalytic domain, and for the C-terminal domain for the simulation of the argifin–ChiB complex. The RMSD values of the catalytic domain and the C-terminal domain reached stable states after about 700 ps, and converged to low values around 1.5 Å. This indicates that the structures of the catalytic domain and the C-terminal domain are well maintained over the MD simulation. By contrast, the RMSD on the whole fluctuated between 1.5 and 3.5 Å. Figure 4A plots the total energy along the MD trajectory of argifin–ChiB complex, indicating that the system was energetically well converged. It suggests that the oscillation of RMSD on the whole was not due to the insufficient simulation time. We found that this behavior was caused by the linker region, because the RMSD on the linker region also varied between 1.5 and 3.5 Å, and the change of the RMSD was correlated between the whole and the linker regions. These results suggest that ChiB displays interdomain motion via the flexible linker region in solution. Figures 3B and 4B also show the RMSD for the simulation of the argadin–ChiB

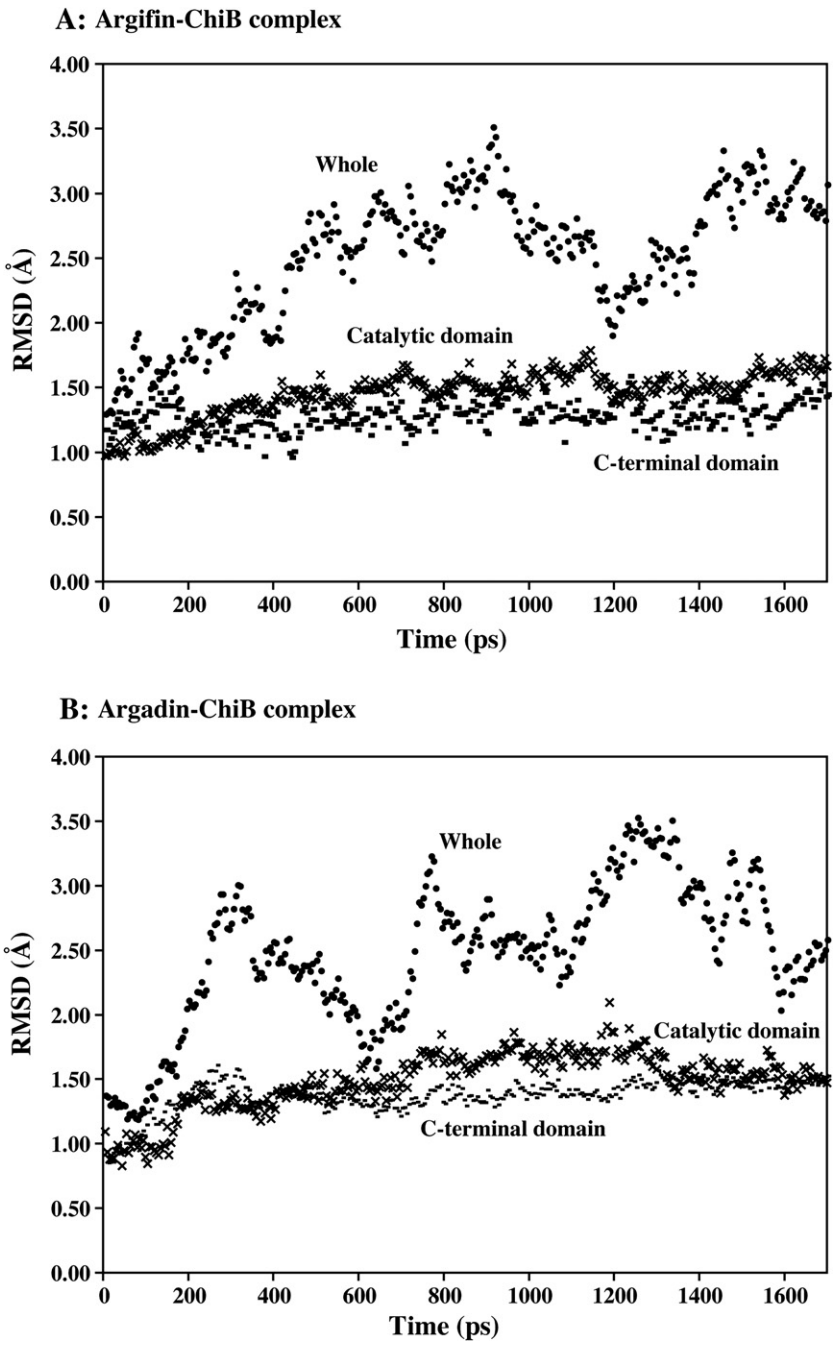

Figure 3. (A) RMSDs relative to the initial structure calculated on the whole, for the catalytic domain of ChiB with argifin, and for the C-terminal domain along the MD trajectory of the argifin–ChiB complex. (B) RMSDs relative to the initial structure calculated on the whole, for the catalytic domain of ChiB with argadin, and for the C-terminal domain along the MD trajectory of argadin–ChiB complex.

complex relative to its initial structure and the total energy along its MD trajectory, respectively. Converged RMSD values were observed on the catalytic domain and the C-terminal domain, but not on the whole. The system was found to be energetically well stable. The interdomain motion was also observed in the argadin–ChiB complex. Our subsequent hydrogen-bonding analysis and MM-PBSA calculation were performed on the last 1000 ps trajectory for each complex.

Figure 5A shows a comparison of the argifin–ChiB complex between the initial structure (X-ray structure) and the final MD structure. The interaction mode observed in the X-ray structure was well retained in the MD simulation. As shown in Figure 2A, five hydrogen bonds were identified between argifin and ChiB in the X-ray structure. The hydrogen-bonding analysis showed that these five hydrogen bonds were well maintained over the MD trajectory (Table 1A). The X-ray structure also indicated one intra-molecular hydrogen bond between L-Asp (**3**) N and D-Ala (**5**) O in the ChiB-bound conformation of argifin (Fig. 2A). This hydrogen bond was again stable over the MD trajectory (Table 1A). In the MD simulation, we found one additional hydrogen

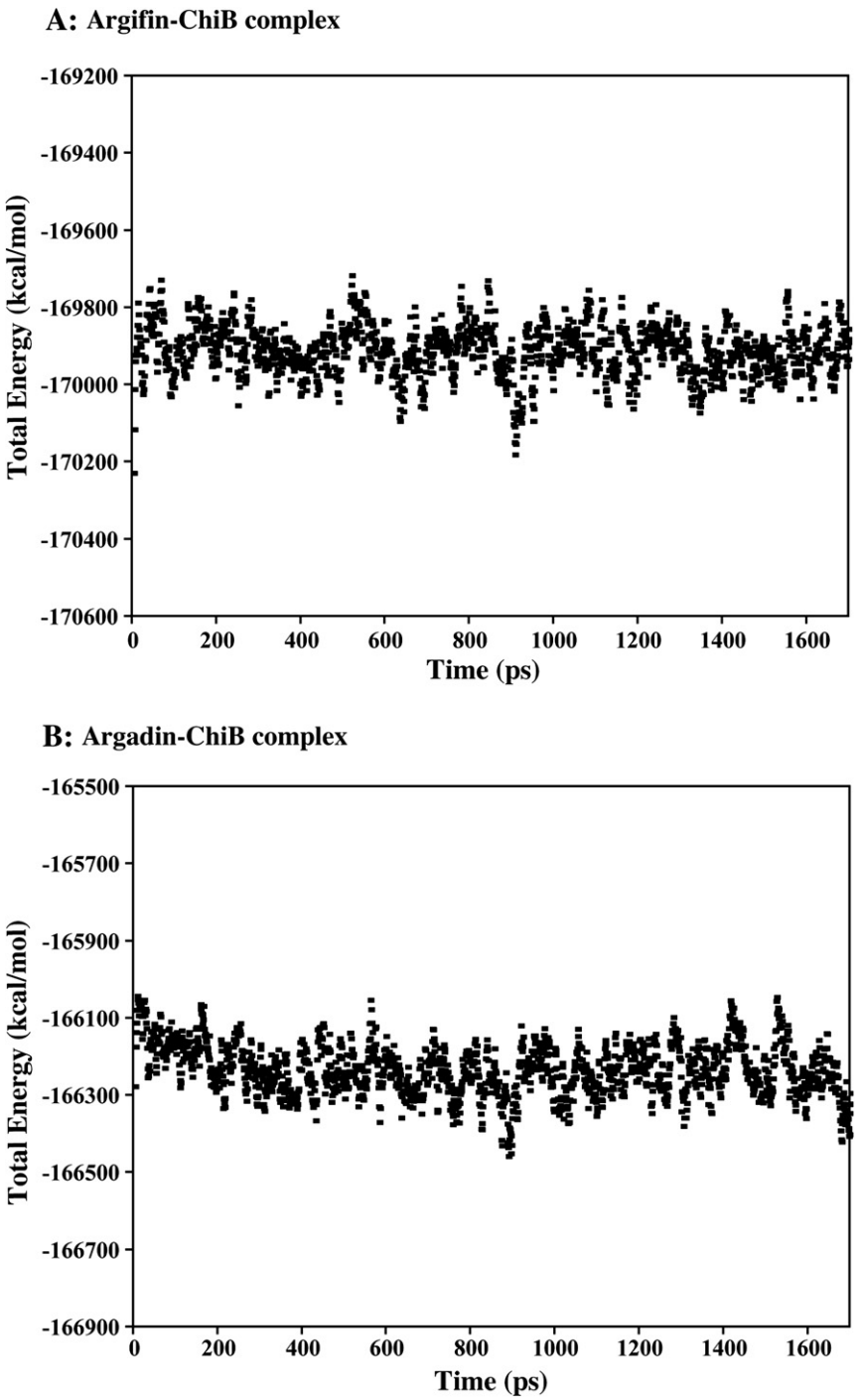

Figure 4. Plots of total energy as a function of simulation time. (A) Argifin–ChiB complex. (B) Argadin–ChiB complex.

bond between the L-Arg (**1**) $N_{\eta 2}$ atom of argifin and the D215 $O_{\delta 2}$ atom of ChiB. Although the distance between these two atoms in the X-ray structure (4.13 Å) was relatively large for a hydrogen bond, it varied between 2.5 and 5.0 Å in the MD simulation. This suggests dynamic hydrogen-bond formation and deformation between these two atoms.

Figure 5B compares the initial structure and the final MD structure on the argadin–ChiB complex, and indicates that the MD simulation has provided a complex that is close to the X-ray structure. In the X-ray structure, the complex had five hydrogen bonds between argadin and ChiB (Fig. 2B). These hydrogen bonds were stable in the MD simulation (Table 1B). The X-ray structure also suggested a total of four intra-molecular hydrogen bonds in the ChiB-bound conformation of argadin (Fig. 2B). Among these four hydrogen bonds, two between the side chains of L-Arg (**1**) and L-aminoadipic acid (**5**) are especially interesting, because these two side chains were located in the hydrophobic pocket consisting of W97, F191, and W220 of ChiB (Fig. 5B).

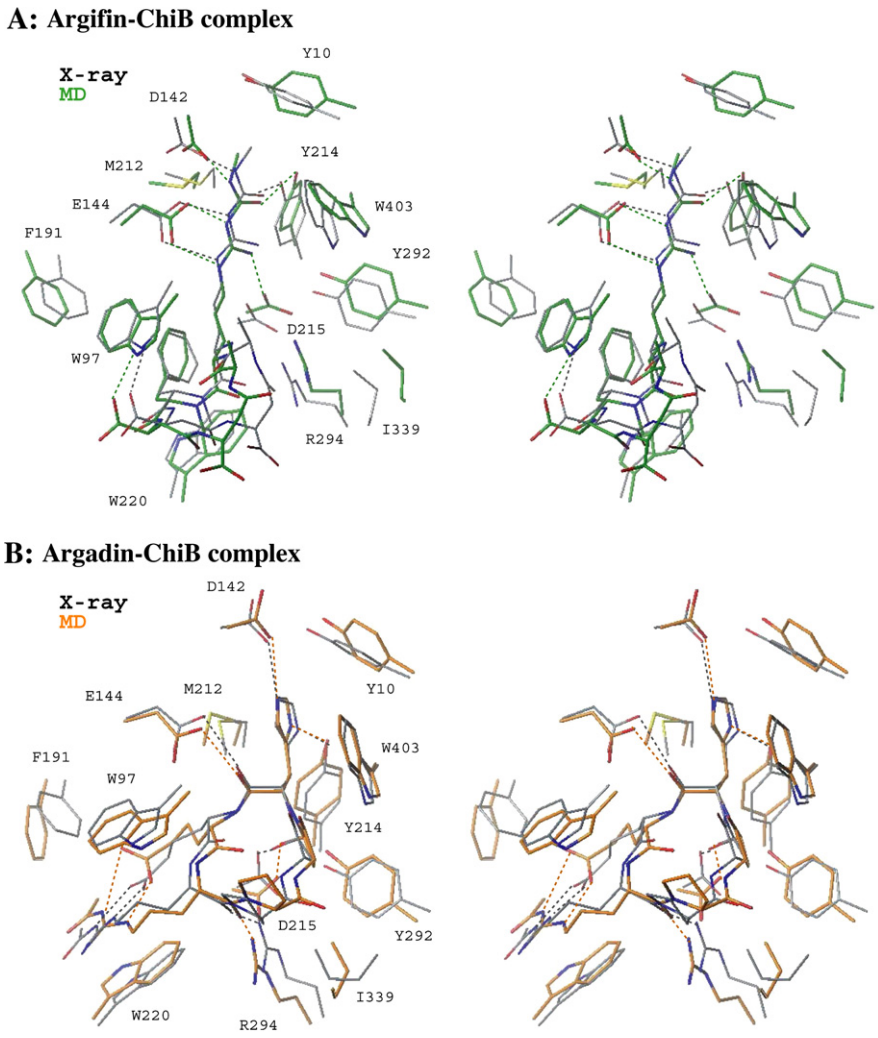

Figure 5. (A) Stereoviews of the superposition of the argifin–ChiB interaction mode in the X-ray structure (gray) and that in the final MD structure (green). The hydrogen bonds in X-ray and MD structures are shown by gray and green dashed lines, respectively. (B) Stereoviews of the superposition of the argadin–ChiB interaction mode in the X-ray structure (gray) and that in the final MD structure (orange). The hydrogen bonds in X-ray and MD structures are shown by gray and orange dashed lines, respectively.

Figure 6 plots the distances between the L-Arg (**1**) C_ζ atom and the L-aminoadipic acid (**5**) C_ε atom along the MD simulation of the argadin–ChiB complex, which was intended to investigate the stability of these two hydrogen bonds. We observed that these two unique hydrogen bonds were well retained throughout the MD trajectory, implying that they were highly stable, and so likely to be of importance in the binding interaction of argadin with ChiB. Two other intra-molecular hydrogen bonds formed between L-aspartic-β-semialdehyde (**3**) and L-aminoadipic acid (**5**) were also maintained over the MD trajectory (Table 1B).

2.2. Structural analysis of argifin and argadin free in solution

Due to the flexible natures of argifin and argadin, their conformations in the bound state might differ greatly from those in the free state in solution. Therefore, we performed separate MD simulations for argifin and argadin, which provide their conformations in the free state. For each simulation, the ChiB-bound conformation taken from the X-ray crystal structure was used as the initial structure. Figure 7A plots the RMSD values relative to the initial structure for the simulation of the free argifin, which were calculated for all heavy atoms. The simulation of free argifin seemed to retain the ChiB-bound conformation, because the RMSD value converged to a low value around 1.0 Å throughout the entire MD trajectory. Figure 8A shows the comparison between the initial structure (ChiB-bound conformation) and the final MD structure, indicating that their structures are similar. In addition, one intra-molecular hydrogen bond observed in the X-ray structure of argifin–ChiB complex was well maintained in the MD trajectory of free argifin (Table 2A). These results suggest that argifin could bind to ChiB without significant conformational change.

The results for the MD simulation of the free argadin are shown in Figures 7B and 8B. In contrast to argifin, the simulation of free argadin seemed to lead to conformations different from the ChiB-bound conforma-

Table 1. Hydrogen-bonding pairs observed in the MD trajectory of complexes

(A) Argifin–ChiB complex

Argifin	ChiB	% Occupied
Inter-molecular H-bonding pair between argifin and ChiB		
Methyl-carbamoyl N	D142 $O_{\delta 2}$	95.8
Methyl-carbamoyl O	Y214 O_{η}	99.9
L-Arg (**1**) N_{ε}	E144 $O_{\varepsilon 1}$	100.0
L-Arg (**1**) $N_{\eta 1}$	E144 $O_{\varepsilon 2}$	100.0
L-Arg (**1**) $N_{\eta 2}$	D215 $O_{\delta 2}$	90.2
L-Asp (**3**) $O_{\delta 1}$	W97 $N_{\varepsilon 1}$	98.9
Argifin	Argifin	% Occupied
Intra-molecular H-bonding pair within argifin		
L-Asp (**3**) N	D-Ala (**5**) O	100.0

(B) Argadin–ChiB complex

Argadin	ChiB	% Occupied
Inter-molecular H-bonding pair between argadin and ChiB		
L-Arg (**1**) O	R294 $N_{\eta 2}$	99.9
L-Aspartic-β-semialdehyde (**3**) $O_{\delta 1}$	D215 $O_{\delta 2}$	100.0
L-His (**4**) $N_{\delta 1}$	Y214 O_{η}	99.6
L-His (**4**) $N_{\varepsilon 2}$	D142 $O_{\delta 2}$	99.5
L-His (**4**) O	E144 $O_{\varepsilon 2}$	99.9
Argadin	Argadin	% Occupied
Intra-molecular H-bonding pair within argadin		
L-Arg (**1**) N_{ε}	L-Aminoadipic acid (**5**) $O_{\zeta 1}$	99.7
L-Arg (**1**) $N_{\eta 1}$	L-Aminoadipic acid (**5**) $O_{\zeta 2}$	99.8
L-Aspartic-β-semialdehyde (**3**) N	L-Aminoadipic acid (**5**) O	99.8
L-Aspartic-β-semialdehyde (**3**) $O_{\delta 1}$	L-Aminoadipic acid (**5**) N	100.0

Hydrogen-bonding analysis was performed using carnal module. Cutoff distance between the heavy atoms is 4.0 Å. Cutoff H-donor–acceptor angle is 60°.

tion, because the RMSD values converged to a larger value around 2.5 Å (Fig. 7B). Figure 8B also shows the dissimilarity between the initial structure (ChiB-bound conformation) and the final MD structure. As shown in Table 2B, three of four intra-molecular hydrogen bonds observed in the ChiB-bound conformation were almost lost in the simulation of free argadin. Figure 6 also shows that the novel two intra-molecular hydrogen bonds between the side chains of L-Arg (**1**) and L-aminoadipic acid (**5**) were not stable in the simulation of free argadin. These results suggest that argadin makes significant conformational changes upon binding to ChiB, and, furthermore, that the binding is dependent upon the formation of these hydrogen bonds.

2.3. Binding free energies calculated by MM-PBSA

In the general MM-PBSA method, the absolute binding free energy is defined as follows:

$$\Delta G_{\text{bind}} = G_{\text{complex}} - (G_{\text{free protein}} + G_{\text{free ligand}}), \quad (1)$$

where, G_{complex}, $G_{\text{free protein}}$, and $G_{\text{free ligand}}$ are the free energies of the complex, the free protein, and the free ligand, respectively.[21] In our calculations, we used the following approximation:

$$G_{\text{free protein}} \approx G_{\text{bound protein}}. \quad (2)$$

This assumes that the protein conformations are similar in the bound and free states. The crystal structure of ChiB in the free state has been reported previously.[32] The free ChiB has D142 in the 'down' position as well as the argadin-bound ChiB. Therefore, we first calculated the RMSD between the free ChiB and the argadin-bound ChiB using a total of 37 residues consisting of the binding site. The calculated RMSD value of 0.66 Å was very small, indicating that the binding site structure of the free ChiB was quite similar to that of the argadin-bound ChiB. Therefore, the approximation of Eq. 2 seems to be adequate for the binding of argadin to ChiB. On the other hand, the RMSD be-

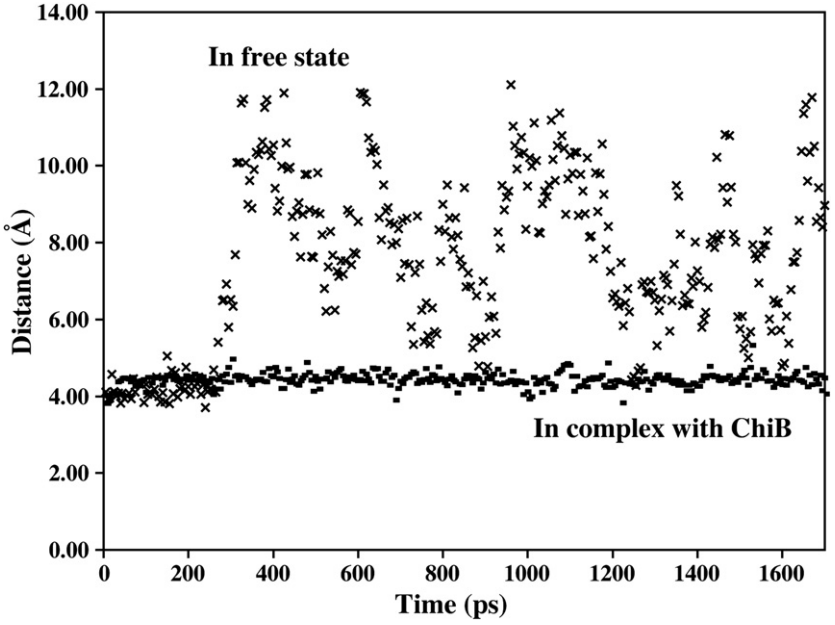

Figure 6. Distances between the L-Arg (**1**) C_{ζ} atom and the L-aminoadipic acid (**5**) C_{ε} atom of argadin both in complex with ChiB and in a free state.

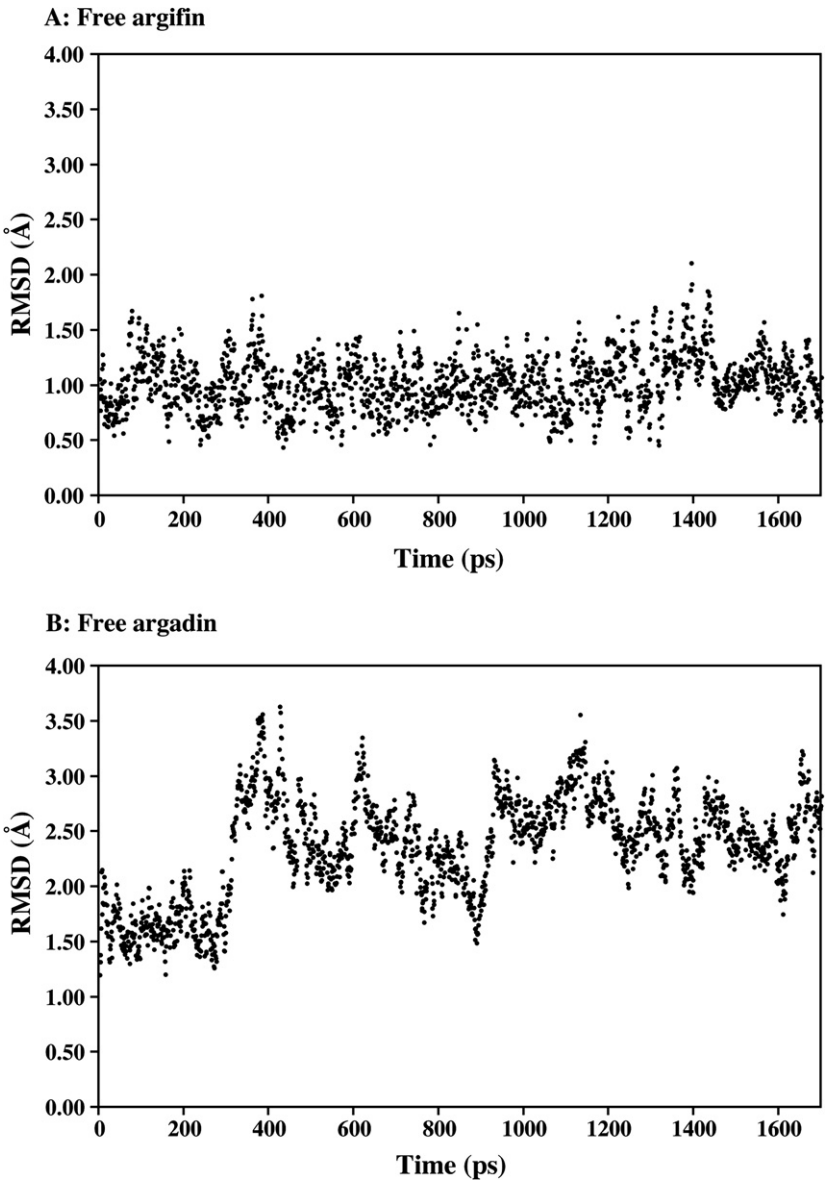

Figure 7. Atom RMSD values from the initial structure as a function of simulation time. (A) MD simulation of the free argifin. (B) MD simulation of the free argadin.

tween the free ChiB and the argifin-bound ChiB was 1.01 Å. The RMSD value was again small, suggesting the structural similarity between the free ChiB and the argifin-bound ChiB, but somewhat larger than that for the argadin-bound ChiB. The structure of free ChiB differs from that of the argifin-bound ChiB by the orientation of the side chain of D142, because D142 is in the 'up' position in the argifin–ChiB complex. This structural difference seems to cause the relatively high RMSD value. Thus, the approximation might not be true for the argifin–ChiB complex. However, in the high-resolution (1.55 Å) crystal structure of the free chitinase A from *S. marcescens* (ChiA),[33] two different kinds of coordinates are given for the side chain of D313, which corresponds to D142 of ChiB. These two conformations correspond to the 'up' and 'down' positions, respectively. This suggests that D313 of the free ChiA could adopt 'up' as well as 'down' orientations, or that the free energy change between them is small. The 'up' orientation of D142 should also be observed in the crystal structure of the free ChiB with higher resolution. Therefore, we consider that the approximation described above is valid for the binding of argifin to ChiB. The estimation of binding free energies using this approximation has been successfully performed for a variety of protein–ligand,[22–26] RNA–ligand,[27] and DNA–ligand[28] interactions.

The results are summarized in Table 3. The absolute binding free energy (ΔG_{bind}) is calculated in the MM-PBSA method as follows:

$$\Delta G_{\text{bind}} = \Delta E_{\text{int}} + \Delta E_{\text{VDW}} + \Delta E_{\text{elec}} + \Delta G_{\text{PB}} + \Delta G_{\text{np}} - T\Delta S, \quad (3)$$

where, ΔE_{int} is the ligand strain defined as the difference in internal energies (bond, angle, and dihedral terms) between the conformation in the bound state

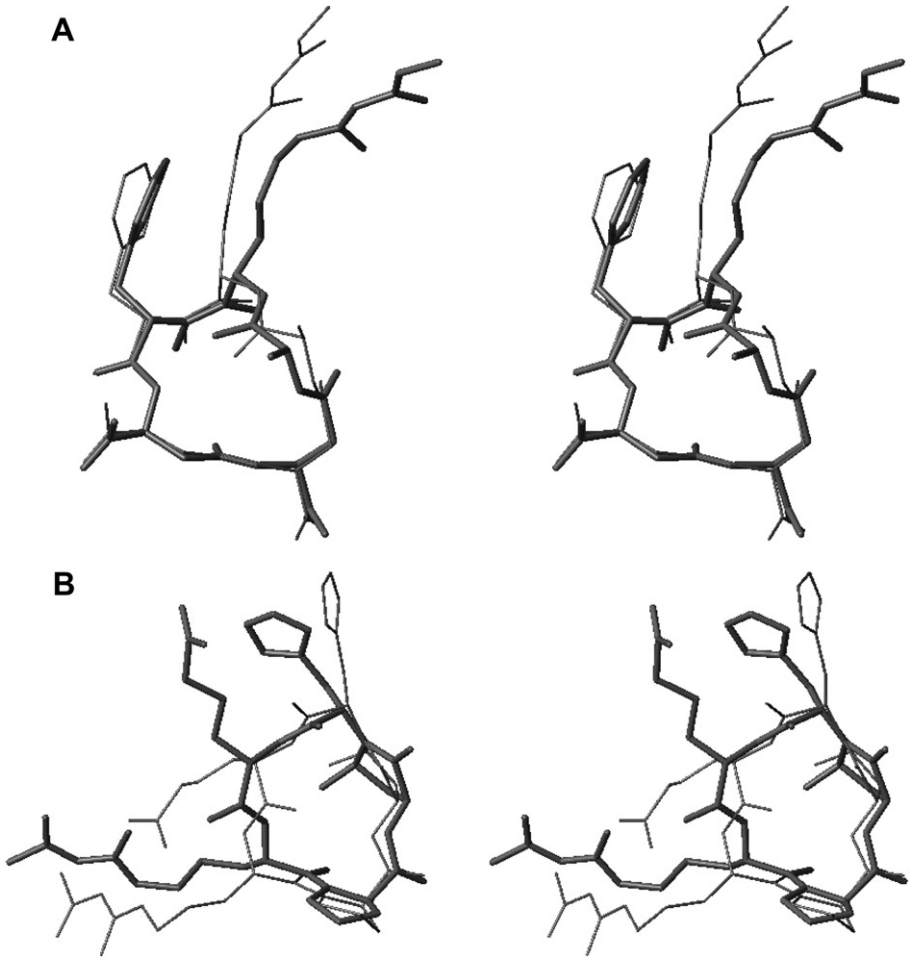

Figure 8. (A) Stereoviews of the superposition of the ChiB-bound conformation of argifin in the X-ray structure (thin line) and the final structure in the MD simulation of free argifin (thick line). (B) Stereoviews of the superposition of the ChiB-bound conformation of argadin in the X-ray structure (thin line) and the final structure in the MD simulation of free argadin (thick line).

and the conformation free in solution; ΔE_{VDW} and ΔE_{elec} terms are the van der Waals and electrostatic interaction energies contributed to binding, respectively; ΔG_{PB} and ΔG_{np} terms are the electrostatic (polar) and nonpolar contributions of solvation free energy to binding, respectively; and $T\Delta S$ is the contribution of solute entropy to binding. The calculated ΔG_{bind} values were −6.98 and −11.16 kcal/mol for argifin and argadin, respectively. These values agreed with those of the experiment[20] (−6.36 and −10.92 kcal/mol for argifin and argadin, respectively), indicating that the MM-PBSA method can reasonably accurately

Table 2. Intra-molecular hydrogen-bonding pairs in the MD trajectory of free ligands

(A) Argifin		% Occupied
L-Asp (**3**) N	D-Ala (**5**) O	99.8
(B) Argadin		
L-Arg (**1**) N_{ε}	L-Aminoadipic acid (**5**) $O_{\zeta 1}$	10.92
L-Arg (**1**) $N_{\eta 1}$	L-Aminoadipic acid (**5**) $O_{\zeta 2}$	6.32
L-Aspartic-β-semialdehyde (**3**) N	L-Aminoadipic acid (**5**) O	0.56
L-Aspartic-β-semialdehyde (**3**) $O_{\delta 1}$	L-Aminoadipic acid (**5**) N	84.4

Hydrogen-bonding analysis was performed using carnal module. Cutoff distance between the heavy atoms is 4.0 Å. Cutoff H-donor–acceptor angle is 60°.

Table 3. Energy contributions (kcal/mol) to the binding free energy of argifin and argadin to ChiB[a]

Contribution	Argifin	Argadin	Difference[j]
ΔE_{int}[b]	0.07 (8.94)	5.26 (10.42)	−5.19
ΔE_{VDW}[c]	−45.06 (5.15)	−57.18 (5.42)	12.12
ΔE_{elec}[d]	4.96 (7.71)	−76.39 (7.40)	81.35
ΔG_{PB}[e]	9.82 (6.77)	94.04 (7.90)	−84.22
ΔG_{np}[f]	−6.55 (0.29)	−7.26 (0.26)	0.71
$-T\Delta S$[g]	29.78 (4.48)	30.37 (4.16)	−0.59
$\Delta G_{(elec,\,tot)}$[h]	14.78 (3.60)	17.65 (3.43)	−2.87
ΔG_{bind}[i]	−6.98 (9.24)	−11.16 (10.75)	4.18
ΔG_{exp}[k]	−6.36	−10.92	4.56

[a] Results are the mean values from 100 (5 in the case of entropy contributions) snapshots. Values in parentheses are standard deviations.
[b] Internal contributions from bond, angle, dihedral terms.
[c] Nonbonded van der Waals.
[d] Nonbonded electrostatics.
[e] Electrostatic component to solvation.
[f] Nonpolar component to solvation.
[g] Entropic contributions to binding.
[h] $\Delta G_{(elec,\,tot)} = \Delta E_{elec} + \Delta G_{PB}$.
[i] Total change of free energy in binding.
[j] Argifin–Argadin.
[k] Experimental data.

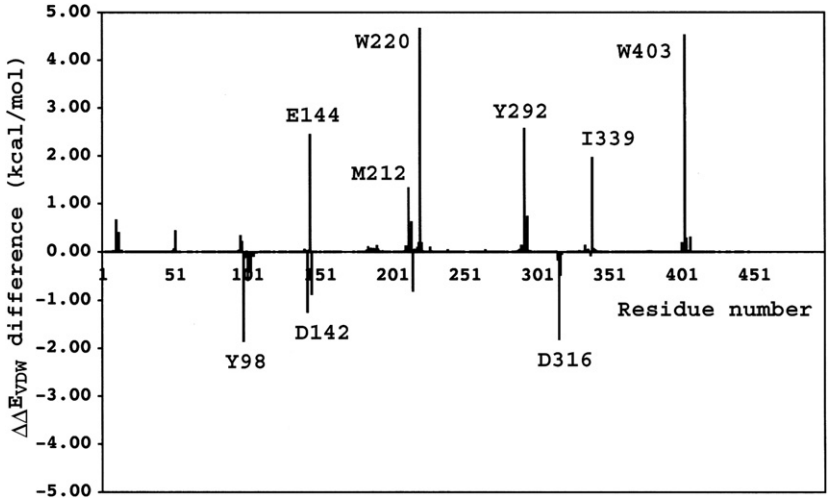

Figure 9. Distribution of the difference of the van der Waals energies between the argifin–ChiB complex and those of the argadin–ChiB complex. Residues with an absolute difference larger than 1.0 kcal/mol are labeled.

reproduce the absolute binding free energies of argifin and argadin complexes. As shown in Eq. 3, the MM-PBSA approach also allowed us to separate the total free energy of binding into some basic components, thereby giving physical insight into the complex association process. The value of ΔE_{int} was almost zero for argifin, indicating that it did not experience a conformational strain upon binding to ChiB. This reflects the observation from the MD simulations that argifin adopts a similar conformation in both bound and free states. By contrast, the MD simulations suggest that argadin requires a conformational change upon binding to ChiB (Fig. 8B). This conformational change has an unfavorable strain energy cost of 5.26 kcal/mol upon binding. As the electrostatic component of the binding free energy ($\Delta G_{(elec,tot)}$) is the sum of the electrostatic interaction energy (ΔE_{elec}) and the electrostatic term in the solvation energy (ΔG_{PB}), this quantity is positive for both argifin and argadin complexes. This indicates that electrostatics oppose the binding of argifin and argadin to ChiB. The favorable formation of these complexes is thus driven solely by the van der Waals contribution and the nonpolar contribution to solvation. This trend is in agreement with numerous other studies using the MM-PBSA method.[22–27]

The calculated relative binding free energy difference ($\Delta\Delta G_{bind}$) of 4.18 kcal/mol was also similar to the experimental value (4.56 kcal/mol). Comparing the contributions to binding between argifin and argadin reveals that the van der Waals and nonpolar solvation energies of argadin are better than the corresponding values observed with argifin. In particular, the van der Waals interaction energies favor the binding of argadin by ~12 kcal/mol compared with argifin. Therefore, the van der Waals interactions are mainly responsible for the difference in binding affinities between argifin and argadin. Accordingly, the van der Waals energies between individual residues of ChiB and argifin (argadin) were calculated, in order to determine which residues of ChiB make a significant contribution to the differential in the van der Waals interaction. Figure 9 shows the subtraction between the van der Waals energies of the argifin–ChiB complex and those of the argadin–ChiB complex. Residues with negative and positive differences have more favorable van der Waals energies with argifin and argadin, respectively. In total, there were nine residues with an absolute difference larger than 1.0 kcal/mol, six of which (E144, M212, W220, Y292, I339, and W403) possessed increased van der Waals energies with argadin. Figure 10 shows a comparison of the final MD structure between the argifin–ChiB complex and the argadin–ChiB complex. D-Pro (**2**) and L-aspartic-β-semialdehyde (**3**) of argadin established contacts with Y292 and I339 of ChiB, whereas argifin had no contact with these residues. Although argadin interacted with E144, M212, and W403 of ChiB using L-aspartic-β-semialdehyde (**3**), L-His (**4**), and L-aminoadipic acid (**5**), argifin only used the side chain of L-Arg (**1**). In the argifin–ChiB complex, *N*-methyl-L-Phe (**2**) of argifin established an aromatic stacking interaction in T-shape geometry with W220 of ChiB, while argadin interacted with W220 using a much larger flat moiety, which was formed by the novel intramolecular hydrogen bonds between the side chains of L-Arg (**1**) and L-aminoadipic acid (**5**). In these ways, six residues of ChiB (E144, M212, W220, Y292, I339, and W403) have more favorable van der Waals energies with argadin. In particular, the van der Waals contributions of W220 and W403 in the argadin complex were more favorable than those in the argifin complex by 4.60 and 4.53 kcal/mol, respectively. The sum of these two values (9.13 kcal/mol) almost accounted for the total van der Waals interaction energy difference of 12.12 kcal/mol between the argifin and argadin complexes in Table 3. This suggested that W220 and W403 play a key role in the potent binding affinity of argadin. It has been reported that the W220A mutant of ChiB binds to argifin and argadin with binding free energies of −4.82 and −7.52 kcal/mol, respectively.[20] Compared with their binding free energies to wild-type ChiB (ΔG_{exp} in Table 3), the W220A mutant shows 1.54 and 3.40 kcal/mol losses

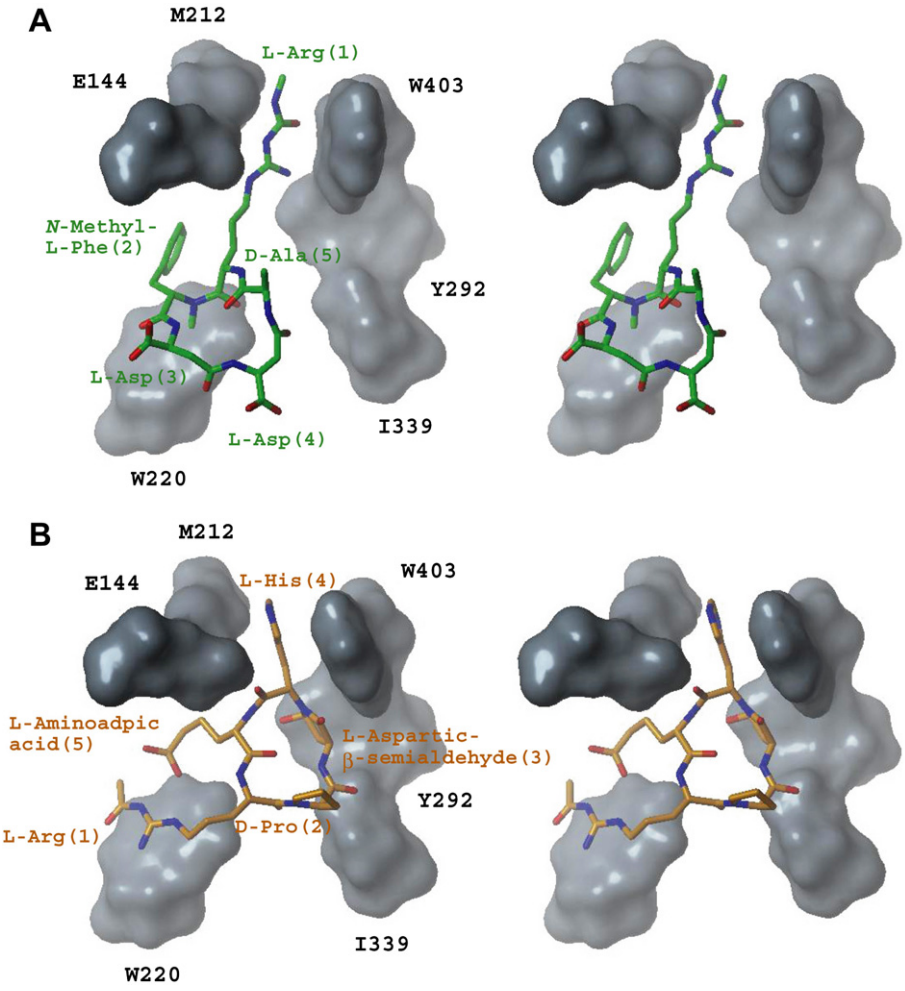

Figure 10. Stereoviews of the final MD structures. (A) Argifin–ChiB complex. (B) Argadin–ChiB complex.

in affinity to argifin and argadin, respectively. The reduction in the binding affinity of argadin is much larger than that of argifin. This experimental result also suggests that W220 is one of the important residues mediating the potent binding affinity of argadin.

2.4. Molecular modeling of argifin derivatives in complex with ChiB

Recently, the total synthesis of argifin has been reported.[34] This encourages us to perform further structure-based inhibitor design. One of our interests is the optimization of argifin, because the binding affinity of argifin is less potent than that of argadin. As described above, the difference of binding affinity between argadin and argifin is mainly due to the van der Waals interaction energies with ChiB. Therefore, one strategy is to design argifin derivatives that would be expected to possess more favorable van der Waals interactions with ChiB. Such argifin derivatives might have a binding affinity with similar potency to that of argadin. Because the *N*-methyl-L-Phe (**2**) of argifin was located in the hydrophobic pocket consisting of W97, F191, and W220 of ChiB (Figs. 5A and 10A), we first considered a derivative in which the *N*-methyl-L-Phe (**2**) was replaced with *N*-methyl-L-Trp, aiming at the increase of the van der Waals interaction. However, we found that the indole ring of Trp was too large to be accommodated in this pocket, because it caused the severe crash with ChiB. Next, our attention was drawn to the D-Ala (**5**) of argifin. Figure 11A shows the final MD structure of the argifin–ChiB complex. There was a wide space to accommodate more bulky side chains around the D-Ala (**5**) of argifin. Therefore, we built modeling structures of argifin derivatives in complex with ChiB, in which the D-Ala (**5**) of argifin was replaced with D-Val, D-Leu, D-Phe, and D-Trp. Figure 11B shows the modeled complex structure between an argifin derivative with D-Trp (**5**) and ChiB. Following the dot surface, the introduced D-Trp (**5**) could occupy the available space and make additional contacts with F51, W97, Y98, and W403 of ChiB. Such a substitution would be expected to improve the van der Waals interaction with ChiB, and so lead to more potent binding affinity than that of wild-type argifin. The relative binding affinities are approximated by single-point MM-PBSA calculations using the minimized complex structures (Table 4). The argifin derivatives with D-Leu (**5**), D-Phe (**5**), or D-Trp (**5**) were expected to have greater free energies of binding than argifin. In particular, the argifin derivative with D-Trp (**5**) would

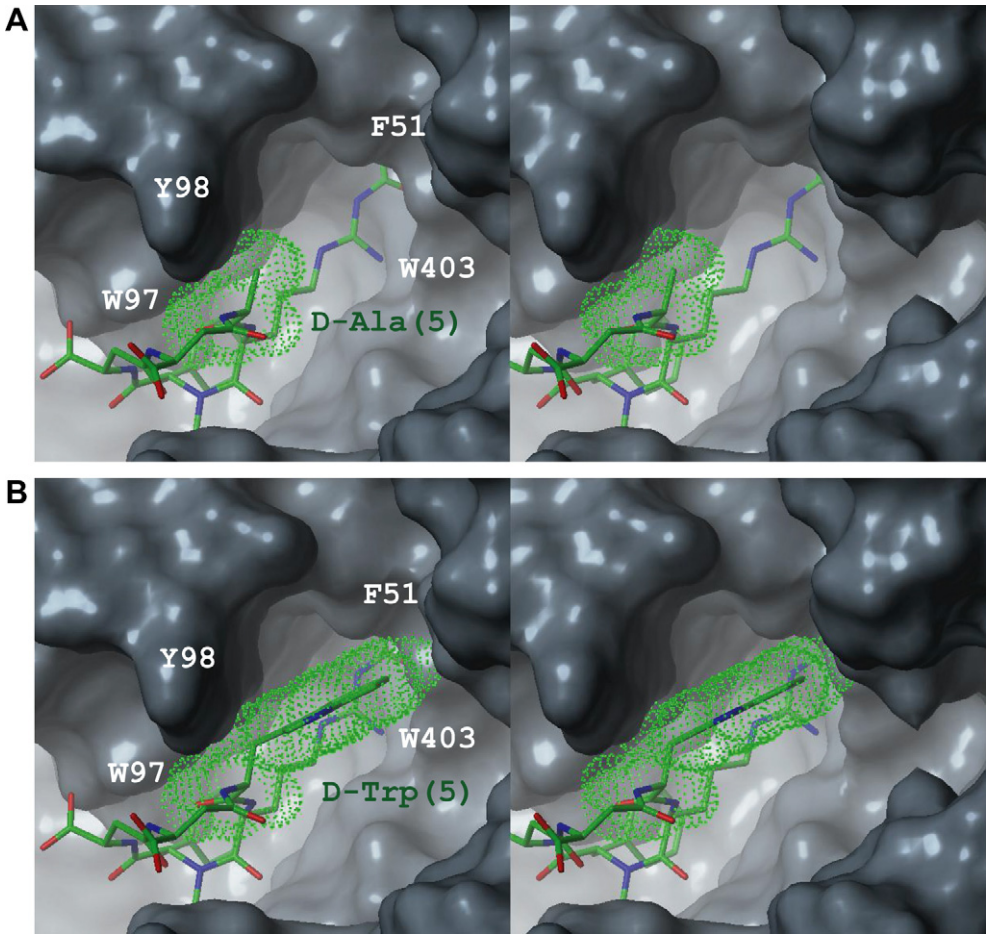

Figure 11. (A) Stereoviews of the final MD structure of the argifin–ChiB complex. The dot surface is given for D-Ala (**5**) of argifin. (B) Stereoviews of the modeling structure of the argifin derivative with D-Trp (**5**) in complex with ChiB. The dot surface is given for D-Trp (**5**).

be expected to gain ~5 kcal/mol more binding free energy in comparison to native argifin. For this argifin derivative, we carried out the MD simulations both in complex with ChiB and in the free state, and then used the MM-PBSA method to estimate the binding free energies more precisely. The results are summarized in Table 5. The binding free energy of the argifin derivative with D-Trp (**5**) was greater than that of argifin by 4.39 kcal/mol. These improvements were mainly due to more favorable van der Waals interactions, as expected (Table 5). It is noteworthy that argadin experimentally binds to ChiB with 4.56 kcal/mol better binding free energy than the wild-type argifin (Table 3). Therefore, the argifin derivative with D-Trp (**5**) might have similar potency to argadin. The synthesis of this derivative is currently underway in our laboratory.

Table 4. Relative binding free energies (kcal/mol) among argifin derivatives estimated by MM-PBSA method

Argifin derivative	ΔG_{bind}[a]	$\Delta\Delta G_{bind}$
Wild-type	−44.60	0.00
D-Ala (**5**) → D-Val (**5**)	−44.03	0.57
D-Ala (**5**) → D-Leu (**5**)	−45.06	−0.46
D-Ala (**5**) → D-Phe (**5**)	−47.73	−3.13
D-Ala (**5**) → D-Trp (**5**)	−49.60	−5.00

[a] Solute entropy term is not included.

Table 5. Energy contributions (kcal/mol) to the binding free energy of the wild argifin and the argifin derivative with D-Trp(5) to ChiB[a]

Contribution	Wild	Argifin derivative D-Ala (**5**) → D-Trp (**5**)	Difference[j]
ΔE_{int}[b]	0.07 (8.94)	1.29 (11.16)	−1.22
ΔE_{VDW}[c]	−45.06 (5.15)	−55.47 (5.30)	10.41
ΔE_{elec}[d]	4.96 (7.71)	9.68 (7.02)	−4.72
ΔG_{PB}[e]	9.82 (6.77)	8.34 (6.34)	1.48
ΔG_{np}[f]	−6.55 (0.29)	−7.18 (0.17)	0.63
$-T\Delta S$[g]	29.78 (4.48)	31.97 (5.35)	−2.19
$\Delta G_{(elec,\ tot)}$[h]	14.78 (3.60)	18.02 (3.10)	−3.24
ΔG_{bind}[i]	−6.98 (9.24)	−11.37 (12.42)	4.39
ΔG_{exp}[k]	−6.36	—	—

[a] Results are the mean values from 100 (5 in the case of entropy contributions) snapshots. Values in parentheses are standard deviations.
[b] Internal contributions from bond, angle, dihedral terms.
[c] Nonbonded van der Waals.
[d] Nonbonded electrostatics.
[e] Electrostatic component to solvation.
[f] Nonpolar component to solvation.
[g] Entropic contributions to binding.
[h] $\Delta G_{(elec,tot)} = \Delta E_{elec} + \Delta G_{PB}$.
[i] Total change of free energy in binding.
[j] Wild-[argifin derivative with D-Trp (**5**)].
[k] Experimental data.

3. Conclusion

We have applied the MM-PBSA method to study the interaction of argifin and argadin with ChiB. Our calculated absolute binding free energies were −6.98 and −11.16 kcal/mol for argifin and argadin complexes, respectively. These were in good agreement with the experimentally determined binding free energies of −6.36 and −10.92 kcal/mol for argifin and argadin complexes, respectively, indicating that this model accurately represents the experimental situation. The energy analysis suggests that argadin takes advantage of increased van der Waals interactions to bind with ChiB better than argifin. In particular, argadin has over 4 kcal/mol more van der Waals interactions with W220 and W403 of ChiB than does argifin, indicating these two residues play a key role in the more favorable binding of argadin. This is consistent with the experimental fact that the W220A mutant of ChiB shows a greater loss in affinity to argadin than it does to argifin. Finally, we suggest that the argifin derivatives, in which D-Ala (**5**) of argifin is mutated to a residue with a bulky side chain, might have better binding affinities. In particular, the argifin derivative with D-Trp (**5**) is expected to have a binding affinity equally potent to that of argadin. If this is realized experimentally, it will provide a firm basis for the structure-based design of novel ligands for future drug development.

4. Materials and methods

4.1. Construction of the initial structures for MD simulations

The conformation of the side chain of D142 is different in the argifin and argadin complexes, as shown in Figure 2. This movement of the D142 side chain is considered to play a key role in the catalytic mechanism of ChiB. A model for the catalytic mechanism has been proposed on the basis of the X-ray crystal structures of the unliganded ChiB and the inactive ChiB-E144Q mutant complexed with an *N*-acetylglucosamine pentamer (substrate).[35] In this model, the resting ChiB has a protonated D142 that points toward D140 to form a hydrogen bond between the two residues (D142 in the 'down' position). E144 is also protonated in the resting ChiB. Binding of substrate causes rotation of the protonated D142 to donate a proton to E144, and so lowers the acid-dissociation constant (pK_a) of E144 (D142 in the 'up' position). The proton released from E144 attacks the glycosidic oxygen of the substrate to promote the formation of the oxazolinium ion intermediate. The hydrolysis of the oxazolinium ion leads to the resting ChiB. Synstad performed a computational analysis of the pK_a values of D140, D142, and E144, the results of which supported the hypothesis that both D142 and E144 are protonated when D142 is in the 'down' position, while only D142 is protonated when it is in the 'up' position.[36] The orientations of D142 in the argifin and argadin complexes correspond to the 'up' and 'down' positions, respectively. Therefore, in our calculations, we assumed that D142 was protonated in both argifin and argadin complexes, while E144 was protonated only in the latter. All other ionizable residues of ChiB were set at their default protonation states at neutral pH. The guanidyl moieties of argifin and argadin were predicted to be positively charged because the experimental pK_a value of acetylguanidine is 8.33.[37] We assigned N_ε-protonation to the histidine side chain of argadin.

4.2. Molecular dynamics (MD) simulations

All of the MD simulations presented in this work were performed using the AMBER7.0 simulation package[31] and the Cornell et al. force field.[38] The AMBER atom types and partial charges are shown for each atom of nonstandard amino acids of argifin and argadin in the Supplementary Fig. S1. These partial charges were obtained using ab initio calculation at the HF/6-31G* level and restraint electrostatic potential (RESP) method.[39] The values for several missing parameters were chosen based on the existing entries in the force field, which are also included in the Supplementary Table S1. The argifin–ChiB and argadin–ChiB complexes were solvated in a box of TIP3P water molecules with a margin of 10 Å along each dimension. A total of five (three) Na^+ ions was added to neutralize the system of argifin–ChiB complex (argadin–ChiB complex). The total numbers of atoms were 70,877 and 69,549 for argifin and argadin complexes, respectively. Each system was equilibrated as follows. In order to relax the water around the solute, the water was minimized for 1000 steps, followed by 35 ps of 310 K MD with 100 kcal/(mol Å^2) restraints on all solute atoms. This was followed by five rounds of 1000 step energy minimizations on the entire system. Harmonic constraints were applied to all heavy atoms with a strength of 100, 25, 5, 1, and 0 kcal/(mol Å^2) at each round. Finally, the system was heated from 0 to 310 K in 40 ps. After this equilibration phase, the production phase followed at 310 K for up to 1700 ps. The MD simulation was carried out at constant pressure (1 atm) and temperature (310 K), under periodic boundary conditions, and with particle-mesh Ewald treatment of electrostatics.[40] SHAKE[41] was applied to all bonds involving hydrogen, and a time step of 1 fs was used. An 8-Å cutoff was used for the nonbonded interactions.

The MD simulations of argadin and argifin in the free state were also performed in order to obtain their solution conformations. The initial coordinates of argadin and argifin were taken directly from their structures complexed with ChiB. The MD simulations of argadin and argifin were performed using the conditions described above. The conformations generated from these MD simulations were used to calculate the free energies associated with the ligands free in solution.

The hydrogen-bonding analysis of MD trajectories was performed using *carnal* module of AMBER 7.0.[31] Cutoff distance between the heavy atoms is 4.0 Å. Cutoff H-donor–acceptor angle is 60°.

4.3. MM-PBSA calculations

The procedure for estimating the binding free energies of argifin and argadin to ChiB was as follows. For each

complex, 100 snapshots were extracted from the last 1000 ps on the MD trajectory with an interval of 10 ps. The coordinates for the unbound ChiB were also taken from the complex trajectory. The unbound conformations of argifin and argadin were obtained from the separate MD trajectories of ligands free in solution. Utilizing these conformations taken from the MD simulations, the MM-PBSA energy analysis was applied to estimate the G_{complex}, $G_{\text{free protein}}$ ($\approx G_{\text{bound protein}}$), and $G_{\text{free ligand}}$. Each of these was calculated by summing the molecular mechanics energy in the gas phase (E_{gas}), the solvation free energy (G_{solv}), and an estimate of the solute entropy (TS_{solute}) as follows:

$$G = E_{\text{gas}} + G_{\text{solv}} - TS_{\text{solute}}.$$

The E_{gas} includes the internal (E_{int}, that is, bond, angle, and dihedral energies), van der Waals (E_{VDW}), and electrostatic (E_{elec}) energies. It is calculated using the AMBER *anal* program without applying a cutoff for nonbonded interactions. The solvation free energy is divided into two parts:

$$G_{\text{solv}} = G_{\text{PB}} + G_{\text{np}}.$$

The G_{PB}, which is the electrostatic contribution to the solvation free energy, was calculated with the PB method as implemented in the Delphi II program.[42] A cubic lattice, which had a grid spacing of 0.5 Å, was 80% filled with the solute. Dielectric constants of 2 and 80 were used for the interior and exterior, respectively. The dielectric boundary was taken as the solvent-accessible surface defined by a 1.4-Å probe radius. The radii of the atoms were taken from the PARSE parameter set.[43] Partial charges were taken from the Cornell et al. force field.[38] In total, 1000 finite-difference iterations were performed to ensure convergence of the results. The nonpolar contribution to the solvation free energy, G_{np}, was calculated by the solvent-accessible surface area (SASA) algorithm of Sanner,[44] where $G_{\text{np}} = \gamma(\text{SASA}) + \beta$ ($\gamma = 0.00542$ kcal/[mol Å^2], $\beta = 0.92$ kcal/mol).[22] The SASA was estimated using the MSMS program[44] with a solvent probe radius of 1.4 Å. Normal-mode analysis was used to estimate the solute entropy. In the absence of solvent, the structures were minimized with no cutoff for nonbonded interactions using the conjugate gradient and then Newton-Raphson minimizations until the root-mean-square of the elements of the gradient vector was less than 10^{-4} kcal/mol. Then, normal-mode calculations were carried out with no cutoff for nonbonded interactions. A distance-dependent dielectric constant ($\varepsilon = 4R_{ij}$) was used to mimic solvent screening. Because this analysis required extensive computer time, only five snapshots were used to estimate the order of magnitude of the solute entropy. Finally, the absolute binding free energy (ΔG_{bind}) was estimated according to Eq. 1.

4.4. Molecular modeling of argifin derivatives in complex with ChiB

The final MD structure of the argifin–ChiB complex was used to model the complex between the argifin derivatives and ChiB. D-Ala (**5**) of argifin was mutated to D-Val, D-Leu, D-Phe, and D-Trp. The orientations of the side chains of these incorporated residues were determined by conformational analysis using the systematic search module of SYBYL6.91 (Tripos, St. Louis, MO, USA). Increments of 15° and 30° were used for the χ_1 and χ_2 dihedral angles, respectively. An energy minimization of 2500 steps was performed for a region of 5 Å around the argifin derivatives using a distance-dependent dielectric constant of $4R_{ij}$. The MM-PBSA method was applied for the energy-minimized complex structures, in order to approximate the affinity of the argifin derivatives to ChiB.

Acknowledgments

This work was supported, in part, by Grant-in-Aid for Scientific Research (C) of the Japan Society for the Promotion of Science [KAKENHI 19590043 (H.G.) and KAKENHI 18590015 (T.S.)], by the Takeda Science Foundation, by the Mochida Memorial Foundation for Medical and Pharmaceutical Research, by Research Fellowships of the Japan Society for the Promotion of Science for Young Scientists (A.S.), and by the Kitasato University Research Grant for Young Researchers (H.G.).

Supplementary data

Supplementary data associated with this article can be found, in the online version, at doi:10.1016/j.bmc.2008.02.017.

References and notes

1. Brurberg, M. B.; Nes, I. F.; Eijsink, V. G. H. *Microbiology* **1996**, *142*, 1581.
2. Kuranda, M. J.; Robbins, P. W. *J. Biol. Chem.* **1991**, *266*, 19758.
3. Merzendorfer, H.; Zimoch, L. *J. Exp. Biol.* **2003**, *206*, 4393.
4. Renkema, G. H.; Boot, R. G.; Muijsers, A. O.; Donker-Koopman, W. E.; Aerts, J. M. F. G. *J. Biol. Chem.* **1995**, *270*, 2198.
5. Boot, R. G.; Blommaart, E. F. C.; Swart, E.; Ghauharali-van der Vlugt, K.; Bijl, N.; Moe, C.; Place, A.; Aerts, J. M. F. G. *J. Biol. Chem.* **2001**, *276*, 6770.
6. Takaya, N.; Yamazaki, D.; Horiuchi, H.; Ohta, A.; Takagi, M. *Biosci. Biotechnol. Biochem.* **1998**, *62*, 60.
7. Cohen, E. *Arch. Insect. Biochem. Physiol.* **1993**, *22*, 245.
8. Ōmura, S.; Arai, N.; Yamaguchi, Y.; Masuma, R.; Iwai, Y.; Namikoshi, M.; Turberg, A.; Kölbl, H.; Shiomi, K. *J. Antibiot.* **2000**, *53*, 603.
9. Izumida, H.; Nishijima, M.; Takadera, T.; Nomoto, A. M.; Sano, H. *J. Antibiot.* **1996**, *49*, 829.
10. Zhu, Z.; Zheng, T.; Homer, R. J.; Kim, Y. K.; Chen, N. Y.; Cohn, L.; Hamid, Q.; Elias, J. A. *Science* **2004**, *304*, 1678.
11. Sakuda, S.; Isogai, A.; Matsumoto, S.; Suzuki, A. *J. Antibiot.* **1987**, *40*, 296.
12. Dickinson, K.; Keer, V.; Hitchcock, C. A.; Adams, D. J. *J. Gen. Microbiol.* **1989**, *135*, 1417.
13. Bortone, K.; Monzingo, A. F.; Ernst, S.; Robertus, J. D. *J. Mol. Biol.* **2002**, *320*, 293.
14. Blattner, R.; Furneaux, R. H.; Lynch, G. P. *Carbohydr. Res.* **1996**, *294*, 29.

15. Kato, T.; Shizuri, Y.; Izumida, H.; Yokoyama, A.; Endo, M. *Tetrahedron Lett.* **1995**, *36*, 2133.
16. Izumida, H.; Imamura, N.; Sano, H. *J. Antibiot.* **1996**, *49*, 76.
17. Tabudravu, J. N.; Eijsink, V. G. H.; Gooday, G. W.; Jaspars, M.; Komander, D.; Legg, M.; Synstad, B.; van Aalten, D. M. F. *Bioorg. Med. Chem.* **2002**, *10*, 1123.
18. Shiomi, K.; Arai, N.; Iwai, Y.; Turberg, A.; Kölbl, H.; Ōmura, S. *Tetrahedron Lett.* **2000**, *41*, 2141.
19. Arai, N.; Shiomi, K.; Yamaguchi, Y.; Masuma, R.; Iwai, Y.; Turberg, A.; Kölbl, H.; Ōmura, S. *Chem. Pharm. Bull.* **2000**, *48*, 1442.
20. Houston, D. R.; Shiomi, K.; Arai, N.; Ōmura, S.; Peter, M. G.; Turberg, A.; Synstad, B.; Eijsink, V. G. H.; van Aalten, D. M. F. *Proc. Natl. Acad. Sci. U.S.A.* **2002**, *99*, 9127.
21. Kollman, P. A.; Massova, I.; Reyes, C.; Kuhn, B.; Huo, S.; Chong, L.; Lee, M.; Lee, T.; Duan, Y.; Wang, W.; Donini, O.; Cieplak, P.; Srinivasan, J.; Case, D. A.; Cheatham, T. E., III *Acc. Chem. Res.* **2000**, *33*, 889.
22. Massova, I.; Kollman, P. A. *J. Am. Chem. Soc.* **1999**, *121*, 8133.
23. Wang, W.; Lim, W. A.; Jakalian, A.; Wang, J.; Wang, J.; Luo, R.; Bayly, C. I.; Kollman, P. A. *J. Am. Chem. Soc.* **2001**, *123*, 3986.
24. Chong, L. T.; Duan, Y.; Wang, L.; Massova, I.; Kollman, P. A. *Proc. Natl. Acad. Sci. U.S.A.* **1999**, *96*, 14330.
25. Huo, S.; Wang, J.; Cieplak, P.; Kollman, P. A.; Kuntz, I. D. *J. Med. Chem.* **2002**, *45*, 1412.
26. Masukawa, K. M.; Kollman, P. A.; Kuntz, I. D. *J. Med. Chem.* **2003**, *46*, 5628.
27. Gouda, H.; Kuntz, I. D.; Case, D. A.; Kollman, P. A. *Biopolymers* **2003**, *68*, 16.
28. Spacková, N.; Cheatham, T. E., III; Ryjácek, F.; Lankas, F.; Van Meervelt, L.; Hobza, P.; Sponer, J. *J. Am. Chem. Soc.* **2003**, *125*, 1759.
29. Kramer, K. J.; Muthukrishnan, S. *Insect Biochem. Mol. Biol.* **1997**, *27*, 887.
30. Fukamizo, T. *Curr. Protein Pept. Sci.* **2000**, *1*, 105.
31. Case, D. A.; Pearlman, D. A.; Caldwell, J. W.; Cheatham, T. E.; Wang, J.; Ross, W. S.; Simmerling, C. L.; Darden, T. A.; Merz, K. M.; Stanton, R. V.; Cheng, A. L.; Vincent, J. J.; Crowley, M.; Tsui, V.; Gohlke, H.; Radmer, R. J.; Duan, Y.; Pitera, J.; Massova, I.; Seibel, G. L.; Singh, U. C.; Weiner, P. K.; Kollman, P. A. *AMBER7*; University of California: San Francisco, 2002.
32. van Aalten, D. M. F.; Synstad, B.; Brurberg, M. B.; Hough, E.; Riise, B. W.; Eijsink, V. G. H.; Wierenga, R. K. *Proc. Natl. Acad. Sci. U.S.A.* **2000**, *97*, 5842.
33. Papanikolau, Y.; Tavlas, G.; Vorgias, C. E.; Petratos, K. *Acta Cryst.* **2003**, *D59*, 400.
34. Dixon, M. J.; Andersen, O. A.; van Aalten, D. M. F.; Eggleston, I. M. *Bioorg. Med. Chem. Lett.* **2005**, *15*, 4717.
35. van Aalten, D. M. F.; Komander, D.; Synstad, B.; Gåseidnes, S.; Peter, M. G.; Eijsink, V. G. H. *Proc. Natl. Acad. Sci. U.S.A.* **2001**, *98*, 8979.
36. Synstad, B.; Gåseidnes, S.; Van Aalten, D. M. F.; Vriend, G.; Nielsen, J. E.; Eijsink, V. G. H. *Eur. J. Biochem.* **2004**, *271*, 253.
37. Albert, A.; Goldacre, R.; Phillips, J. *J. Chem. Soc.* **1948**, *70*, 2240.
38. Cornell, W. D.; Cieplak, P.; Bayly, C. I.; Gould, I. R.; Merz, K. M., Jr.; Ferguson, D. M.; Spellmeyer, D. C.; Fox, T.; Caldwell, J. W.; Kollman, P. A. *J. Am. Chem. Soc.* **1995**, *117*, 5179.
39. Cieplak, P.; Cornel, W. D.; Bayly, C.; Kollman, P. A. *J. Comput. Chem.* **1995**, *16*, 1357.
40. Darden, T.; York, D.; Pedersen, L. *J. Chem. Phys.* **1993**, *98*, 10089.
41. Ryckaert, J. P.; Ciccotti, G.; Berendsen, H. J. C. *J. Comput. Phys.* **1977**, *23*, 327.
42. Honig, B.; Nicholls, A. *Science* **1995**, *268*, 1144.
43. Sitkoff, D.; Sharp, K. A.; Honig, B. *J. Phys. Chem.* **1994**, *98*, 1978.
44. Sanner, M. F.; Olson, A. J.; Spehner, J. C. *Biopolymers* **1996**, *38*, 305.